JOURNAL OF GEOPHYSICAL RESEARCH, VOL. 112, A05215, doi:10.1029/2006JA012007, 2007

Large parallel electric fields, currents, and density cavities in dispersive Alfvén waves above the aurora

C. C. Chaston,[1] A. J. Hull,[1] J. W. Bonnell,[1] C. W. Carlson,[1] R. E. Ergun,[2] R. J. Strangeway,[3] and J. P. McFadden[1]

Received 7 August 2006; revised 22 November 2006; accepted 15 January 2007; published 24 May 2007.

[1] Large parallel electric fields ($E_{\|} > 10$ mV/m) are sometimes observed with intense filamentary field-aligned currents ($J_{\|} > 10$ μA/m^2 mapped to 100-km altitude) on transverse scales where $k_x c/\omega_{pe} \approx 1$ above the auroral oval. The ratio of the transverse electric (E_x) and magnetic field (B_y) variations is approximately the local Alfvén speed and increases with decreasing transverse scale in a manner consistent with inertial Alfvén wave dispersion. These fields are typically observed in association with density cavities. Statistically, it is shown that the depth of the cavities observed over the altitude range from 350 to 4175 km by the Fast Auroral Snapshot (FAST) satellite typically lies between 30 and 50% of the background plasma with 90% depletions being observed for 1% of the recorded events. The wave currents embedded within these cavities exceed 100 μA/m^2 for 2% of the ensemble and are typically found over transverse widths of $\sim 2\pi\lambda_e$. Using a fluid description of the plasma, we show statistically that electron pressure gradients provide a probable means for balancing the large $E_{\|}$ found in these structures with a likely but unknown contribution from anomalous resistivity. Furthermore, we find that the ratio of the average drift speed of the bulk electron plasma (v_d) to the electron thermal speed (v_e) inside these structures is $v_d/v_e \geq 0.1$ and that in at least 2% of cases $veh05_d/v_e \geq 1.0$. On the basis of recent simulation results and the Bohm criterion for double layer formation, these statistics indicate that the large $E_{\|}$ sometimes observed in density cavities may occur in double layers driven by the Alfvén wave current.

Citation: Chaston, C. C., A. J. Hull, J. W. Bonnell, C. W. Carlson, R. E. Ergun, R. J. Strangeway, and J. P. McFadden (2007), Large parallel electric fields, currents, and density cavities in dispersive Alfvén waves above the aurora, *J. Geophys. Res.*, *112*, A05215, doi:10.1029/2006JA012007.

1. Introduction

[2] Large parallel electric fields are sometimes observed in Alfvénic field structures above the auroral oval [*Stasiewicz et al.*, 1997; *Chust et al.*, 1998; *Chaston et al.*, 1999; *Ergun et al.*, 2005]. These fields may be balanced by a number of effects which may be formalized in a two-fluid model of the plasma. From the momentum equation for isotropic electrons, the parallel electric field is given by

$$E_{\|} = \frac{m_e}{q_e^2}\frac{dJ_{\|}/n_e}{dt} + \frac{m_e}{q_e^2 n_e}\nu J_{\|_e} + \frac{1}{q_e n_e}\nabla_{\|}P \qquad (1)$$

where q_e is the electron charge (including sign), m_e is the electron mass, n_e is the electron density, $J_{\|}$ is the parallel electron current, P_e is the electron pressure, and ν is an anomalous collision frequency. The assumption of isotropic electrons means we ignore the contribution due to the mirror force. Relative to the other terms, this contribution remains small even in the presence of significant electron anisotropy provided the parallel scale ($\Delta S_{\|}$) is short relative to the parallel gradient scale of the geomagnetic field [*Hull et al.*, 2003]. In the case we consider here, the energy of accelerated electrons observed is generally less than 1 keV, and so the large amplitude parallel fields ($E_{\|} > 10$ mV/m) observed in these waves requires $\Delta S_{\|} < 100$ km. This parallel scale length is much less than the scales over which the geomagnetic field varies.

[3] It has been shown [*Lysak and Carlson*, 1981; *Streltsov et al.*, 2002] that each of the terms on the right-hand side of equation (1) becomes important over specific altitude ranges on an auroral field line. Over the Fast Auroral Snapshot (FAST) altitude range (350–4175 km), the electron thermal speed is generally less than the Alfvén speed (i.e., $v_e < V_A$), and the first term describing the effect of finite electron mass (electron inertia) becomes important [*Lysak and Lotko*, 1996]. Since $J_{\|}$ varies in space and time, this term has a linear and nonlinear contribution through the convective deriva-

[1]Space Sciences Laboratory, University of California, Berkeley, California, USA.
[2]Laboratory for Atmospheric and Space Physics, University of Colorado, Boulder, Colorado, USA.
[3]Institute for Geophysical and Planetary Physics, University of California, Los Angeles, California, USA.

0148-0227/07/2006JA012007$09.00

tive. Assuming periodic fluctuations at frequency ω, the linear field is given by

$$E_{\|t} = -i\omega\mu_o\lambda_e^2 J_\| \quad (2)$$

where λ_e is the electron inertial length or skin depth given by c/ω_{pe}. We note that $E_{\|t}$ given by this expression is 90° out of phase with $J_\|$ and that ω in this relation can be replaced by $\omega = V_A k_\|(1 + k_x^2\lambda_e^2)^{-1/2}$, where k_x and $k_\|$ are the wave numbers transverse and parallel to B_o, respectively. This contribution to $E_\|$ has been used with success to account for electron acceleration in Alfvén waves over this altitude range [*Thompson and Lysak*, 1996]. However, because the parallel wavelengths of Alfvén waves above the aurora are larger than 100 km, and for the largest observed current magnitudes ($\sim$100 μA/m^2) and lowest densities ($\sim$1 cm^{-3}) $E_{\|t} < 2$ mV/m, we can immediately eliminate this term as a candidate to account for observations of $E_\| >$ 10 mV/m which are the topic of this study.

[4] Alternatively, electron inertia can support large $E_\|$ through the convective term which is given by

$$E_{\|v} = (\mu_o/q_e)\lambda_e^2 J_\| \nabla_\| (J_\|/n_e) \quad (3)$$

and has been discussed in the context of auroral particle acceleration by *Lysak and Dum* [1983], *Seyler et al.* [1995], *Ronnmarck and Hamrin* [2000], *Streltsov et al.* [2002], and *Wright et al.* [2002]. The convective derivative is really in terms of v_d; however, we present this as $J_\|/n_e$ to emphasize that this gradient may be manifest through changes in $J_\|$ over large parallel scales and/or in n_e over scales that can be much less than an Alfvén wavelength.

[5] The parallel field due to the second term in equation (1) describes the effect of anomalous collisions and can be written as

$$E_{\|r} = \nu\mu_o\lambda_e^2 J_\| \quad (4)$$

[6] For large $J_\|$ and small n_e, the parallel drift (v_d) of the electrons carrying $J_\|$ can exceed the threshold for various instabilities leading to the formation of a turbulent layer. In general, $\nu \propto k_{\|turb} v_e (q_e V_{\|turb}/T_e)^2$ where $k_{\|turb}$ and $V_{\|turb}$ are characteristic wave numbers and field-aligned potentials of the turbulence giving rise to the resistivity. Because ν in these models is generally much larger than the Alfvén wave frequency (ω), $E_{\|r}$ from equation (4) will generally be much larger than $E_{\|t}$ given by equation (2) once the appropriate instability threshold has been exceeded. Consequently, the resistivity provided by these instabilities is a candidate for supporting large $E_\|$. However, the existing models for ν are generally derived for Maxwellians [e.g., *Lysak and Dum*, 1983] and are not strictly applicable to the distributions we observe. Consequently, in this manuscript, we are unable to quantitatively evaluate the importance of anomalous collisions in accounting for the large $E_\|$ we observe; however, it seems likely that such effects may be important.

[7] The third term on the right in equation (1) represents $E_\|$ supported by a field-aligned pressure gradient. In the linear approximation, this term becomes time-dependent through small field-aligned oscillations in density with $E_{\|Pe} = -i\mu_o/\omega\rho_s^2 V_A^2 \nabla_\|^2 J_\|$ where $\rho_s = v_s/\Omega_i$ is the ion acoustic gyroradius and $v_s = (T_e/m_i)^{1/2}$ is the ion acoustic speed [*Hasegawa*, 1976]. In the local approximation, the ratio of $E_{\|t}$ given by equation (2) and that due to the electron pressure gradient becomes $\sim\lambda_e^2/\rho_s^2$. At the altitudes traversed by FAST, we find generally that $\lambda_e > \rho_s$, and so the pressure gradient contribution balancing $E_\|$ can be ignored. This, however, is not necessarily the case if zero-order gradients in P_e exist in the ambient plasma. The ratio of the electron inertial and pressure contributions to $E_\|$ is then

$$\frac{E_{\|v}}{E_{\|Pe}} = \frac{m_e n_e}{2}\left(\frac{\partial v_d^2/\partial S_\|}{\partial P_e/\partial S_\|}\right) \quad (5)$$

[8] If v_d and P_e vary over parallel scales $\Delta S_\| v$ and $\Delta S_{\|Pe}$, respectively, then this ratio becomes $\sim(v_d^2\Delta S_{\|Pe})/(v_e^2\Delta S_{\|v})$ [*Hull et al.*, 2003]. For field-aligned currents over large parallel scales, v_d will generally be less than v_e because of strong instability preventing $v_d \approx v_e$. So if $\Delta S_{\|Pe} \approx \Delta S_{\|v}$, the pressure term will dominate. However, for the case of parallel scales much less than an Alfvén wavelength, v_d may approach or even exceed v_e [*Andersson et al.*, 2002] leading to the formation of double layers [*Raadu and Rasmussen*, 1988]. In the fluid approximation, this is the Bohm criteria for double layer formation [*Block*, 1972]. Since these features have parallel scales of the order of Debye lengths (λ_D) and form on timescales of the order of several ion plasma periods (<0.005 s and much less than an Alfvén wave period), they may be considered independently as electrostatic structures driven by the current of the Alfvén wave which is partially dissipated through particle acceleration and heating within the double layer [*Silberstein and Otani*, 1994].

[9] The description given above identifies the means through which large parallel electric fields in Alfvén waves may be locally supported. Over the small parallel scales where such fields exist, this may be achieved either through electron inertia, anomalous resistivity, or via electron pressure gradients. Alternatively, nonlocal kinetic models have been developed [*Rankin et al.*, 1999; *Lysak and Song*, 2003; *Vedin and Ronnmarck*, 2005]. These include the effect of magnetic mirroring and the field-aligned homogeneity of the plasma to show that over parallel scales of the ionospheric Alfvén resonator or field-line resonances, significantly larger $E_\|$ than given by the local description may occur. Such effects will be important for parallel fields established over periods longer than an electron transit time through a parallel Alfvén wavelength. However, these considerations may not be necessary to understand to first order how the large amplitude fields we consider here ($E_\| >$ 10 mV/m) are supported. This is because the parallel scales we consider ($\Delta S_\| <$ 100 km) are generally much less than an Alfvén wavelength, and an electron transit time through these scales is much less than an Alfvén wave period. Consequently, we believe that the local treatment is sufficient to evaluate the means by which large parallel fields are locally balanced.

[10] Notably the magnitude of the parallel electric field given by all the terms in equation (1) vary inversely with n_e and, with the exception of pressure gradients, increase with increasing $J_\|$. Consequently, it is not surprising that large

parallel fields in Alfvén waves occur in density depletions with large $J_{\|}$. In this manuscript, we first present a case study example of an Alfvén wave carrying large $J_{\|}$ imbedded in a density cavity where large $E_{\|}$ is observed and show that this field exists in background of inertial Alfvén wave turbulence. We then statistically report observations of similar cavities containing large field-aligned currents carried by Alfvén waves where large $E_{\|}$ can be expected to exist. These observations are then used to estimate the field-aligned potentials that may be supported by electron inertia and electron pressure gradients inside these density cavities according to the equations given above. We note that nearly all the events we have inspected visually contain electric field vectors which may have a substantial $E_{\|}$ component. However, since it is notoriously difficult to reliably identify and measure parallel electric fields in an automated manner, we do not report statistical measurements of $E_{\|}$. We also do not attempt to address the causality of these fields as addressed by *Song and Lysak* [2006].

2. Case Study Example

2.1. Fields and Particle Observations

[11] Figure 1 shows observations from the FAST satellite recorded above the auroral oval during an interval when Alfvénic fluctuations in field quantities were observed. The configuration and orientation of the FAST electric field instrument relative to the projection of the geomagnetic field (B_o) into the spin plane (B_{sp}) is shown in Figure 1a at 13:55:20.55 UT. This configuration provides multiple dipole pairs from which **E** in the spin plane can be measured. This measurement is transformed into a "near-field-aligned" nonrotating coordinate system where E_x is orthogonal to B_o and points roughly northward and E_z is along B_{sp}. The third, and unmeasured, component of E (E_y) lies along the spacecraft spin axis. Since B_o lies within 2.4° of B_{sp}, then in the absence of large E_y, we find that $E_z \approx E_{\|}$. The largest fields measured above the aurora have magnitudes up to ~1 V/m and are only occasionally measured [*Ergun et al.*, 1998]. If these fields were along E_y, they would contribute 40 mV/m to $E_{\|}$. Consequently, we imposed a conservative reliability threshold of 40 mV/m on E_z when equating E_z with $E_{\|}$.

[12] Figures 1b and 1c show that E_x contains fluctuations over a range of frequencies in the spacecraft frame (f_{sp}) with spectral peaks apparent just below and above the oxygen (f_{O+}) cyclotron frequency with $f_{sp} \approx 0.9f_i$ and $1.5f_i$ (where f_i

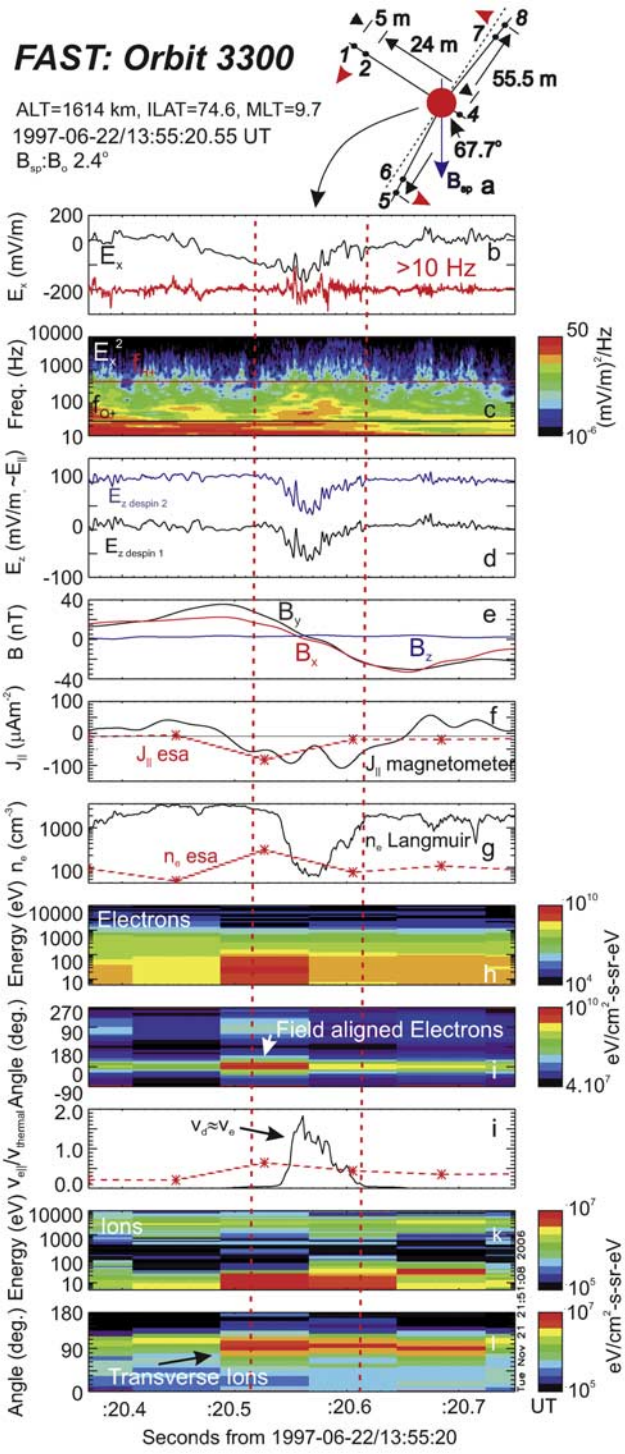

Figure 1. (a) Orientation of the FAST spacecraft when large $E_{\|}$ is observed. (b) Electric field perpendicular to B_o and pointing northwards (E_x). The red trace shows variations at frequencies above 10 Hz. (c) Spectral energy density of electric field fluctuations. (d) Approximate parallel electric field (E_z). The black and blue traces show the electric field along the projection of B_o into the spin plane (B_{sp}) using measurements from spin plane dipole pairs 1–4 and 5–8, and 1 − (5 + 8)/2 and 5–8, respectively. The blue trace has been shifted by 100 mV/m and the spin plane lies within 2.4° of B_o. (e) Perturbed magnetic field. (f) Field-aligned current as measured from spatial gradients in B (black) and by the electrostatic analyzer (esa) above 5 eV (red). (g) Electron number density as measured from a calibrated Langmuir probe (black) and from the electrostatic analyzer (red). (h, i) Electron energy and pitch angle spectrograms with 0° being downwards along B_o. (j) Ratio of electron drift speed (v_d) to thermal speed (v_e) with v_d from the observed current (black) and from the electron spectrometer (red). (k, l) Ion energy and pitch angle spectrograms with 90° being transverse to B_o and opposite to the satellite motion.

is the gyrofrequency based on the average ion mass). These peaks are superimposed on a broader background spectrum extending through the hydrogen (f_{H+}) cyclotron frequency. The spectral density of these fluctuations is enhanced from 13:55:20.51 to 13:55:20.61 between the red lines and where Figure 1d shows a substantial E_z component. Because measurements of $E_\parallel$ (and hence E_z) are subject to significant experimental uncertainty, we provide two semi-independent measurements of E_z. The black trace in Figure 1d shows E_z determined from the relative potential between the orthogonal probe pairs 1–4 and 5–8, while the blue trace shows the same measurement but with the 1–4 measurement replaced by the relative potential between probe 1 and the average from probes 5 and 8 (which has been shifted by 100 mV/m in Figure 1d for visibility). Both measurements provide almost identical results. Furthermore, E_z reaches an amplitude of 60 mV/m which is above the 40 mV/m threshold. This indicates that E_z over the interval from 13:55:20.51 to 20.61 UT is a reliable measurement of an upward pointing (negative) $E_\parallel$.

[13] Figure 1e shows that over this interval, the magnetic field is perturbed transverse to B_o in both B_x and B_y. It has been shown elsewhere [*Stasiewicz et al.*, 2000] and has been verified for this case study using interferometry (see section 2.2) that at this altitude, much of the perpendicular temporal structure observed in the magnetic field is due to spacecraft Doppler shift. Thus Ampere's law can be used to evaluate the current density directly from the observed gradients in B under the assumption that the structure is time stationary over the satellite transit time. From a variance analysis, the geometry of the magnetic field measurements is consistent with the traversal of three adjacent field-aligned current sheets inclined at 45–60° to the spacecraft trajectory. This is shown in Figure 1f by the black trace indicating positive (downward), then negative (upward), and then positive $J_\parallel$. The central upward current reaches 100 μA/m^2 at 13:55:20.59 UT and has a width of $\sim 2\pi c/\omega_{pe}$. This current bounds the peak in E_z shown in Figure 1d and yields $J_\parallel E_\parallel \leq 6 \times 10^{-3}$ mW/m^3. As indicated by the red trace in Figure 1f, $J_\parallel$ for the total plasma given by gradients in B is colocated with, and of similar magnitude to, the current in the energetic plasma as measured by the particle instrument above 5 eV. It is also coincident with a depletion or cavity in the ionospheric plasma shown in Figure 1g derived from the Langmuir probe current. This instrument has been calibrated using emissions at ω_{pe} adjacent to the cavity (within the cavity, an emission at ω_{pe} is not observed and so there is some uncertainty in the actual depth). Conversely, the density as measured by the particle instrument, and shown here by the red trace in Figure 1g, reveals enhanced densities of energetic plasma (>5 eV) in the vicinity of the depletion. These observations suggest that the cavity is formed by a depletion of cold plasma at energies below the 5-eV lower limit of the particle experiment in a region of large field-aligned current density.

[14] The remaining panels of Figure 1 show that the observed parallel electric field structure is localized to a region of field-aligned electron and transverse ion acceleration. Figures 1h and 1i show that the enhanced energetic densities/electron fluxes observed within the density cavity occur at energies below 100 eV and are downgoing along the geomagnetic field with pitch angles within a few degrees of B_o. As shown in Figure 1j, the average earthward drift speed of these electrons is of the same order as their thermal speed. These curves show v_d/v_e evaluated using v_e from energetic electron population measured above 5 eV, and v_d using, in one case, the current given by the magnetometer (black trace) and, in the other, the velocity moment from the electron analyzer (red trace). While the electron measurements do not completely resolve the structure, this measurement is consistent with the Bohm criteria in the fluid approximation [*Block*, 1972] for the existence of double layers. These field-aligned electrons are observed coincident with transversely accelerated ions as shown in Figures 1k and 1l. The ions are nearly exactly perpendicular to B_o suggestive of local transverse acceleration within the electric field structure. Also, the ion loss cone feature at 150°–180° becomes partially filled over the interval where the parallel electric field is observed. These field-aligned ions, together with the transversely accelerated ions, provide a net upward ion flux out of the parallel electric field region. These particle observations are indicative of a region localized in altitude from which electrons are accelerated downward and ions transversely and upward.

[15] By considering the delay time between measurements made from each of the dipole pairs shown in Figure 1a, it is possible to determine the trajectory of the parallel field structure in the spacecraft spin plane. This technique is described in Appendix A. Using this approach, and averaging the time delays observed over the region between the red lines in Figure 1, we find that the parallel electric field structure travels down the geomagnetic field with a speed of 16.4 km s^{-1} ($v_{ion\_thermal} \approx v_s \approx 13$ km s^{-1}) and southward transverse to B_o with a speed of 7.6 km s^{-1} (note that the spacecraft velocity has been subtracted from these numbers, and so they represent speeds in the rest frame). Consequently, under the assumption that the structures does not vary temporally over the interval of observation, the region between the red dashed lines corresponds to a slice through the electric field structure of length ~1.6 km along B_o ($\lambda_D \approx 5$ m inside the cavity) and ~760 m transverse. This slice in the frame of the electric field structure is shown in Figure 2a. The vectors given in Figure 2a indicate the orientation of the equipotentials along this slice with their length representing the magnitude of the electric field observed. The blue and red lines in this panel show the integrated parallel and perpendicular potentials through this structure. These are derived by integrating the observed parallel and perpendicular electric fields along the parallel and perpendicular components of satellite trajectory. We find that the parallel potential traversed by the FAST satellite is $\sim V_\parallel \approx 44$ V, while the perpendicular potential is $V_\perp \approx 43$ V. The parallel potential is consistent with energy of the electrons shown in Figure 1h.

[16] Figures 2b and 2c show the electron distributions observed above (upstream) and below (downstream) the parallel electric field structure. In the upstream region, there is evidence of preacceleration perhaps in similar field structures at higher altitudes. Comparing the upstream and downstream measurements, the acceleration by the parallel electric field is clearly apparent with a significant enhancement in field-aligned phase space densities. The electron energy flux observed in the downstream distribution is 1.5 mW/m^2. Using the observed parallel scale, and inte-

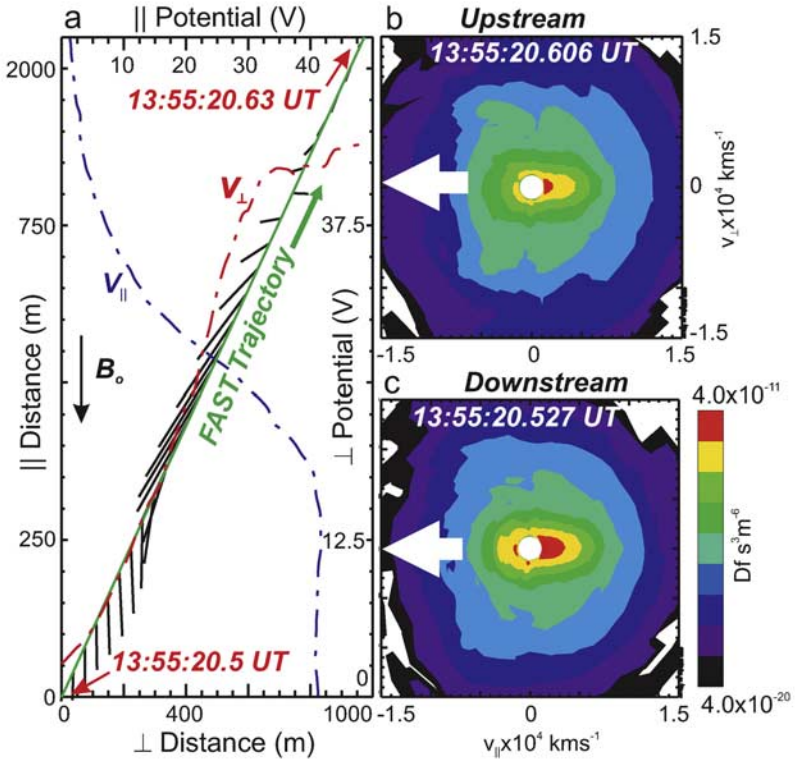

Figure 2. FAST's trajectory through the electric field structure. (a) Trajectory of the FAST satellite in the frame of the electric field structure (green line). Black lines show the orientation of the equipotentials traversed along this trajectory with length equal to the total electric field magnitude at that point. The red dashed line shows the perpendicular potential (secondary y axis) along the spacecraft trajectory as a function of $\perp$ position (x axis). The blue dashed line shows the parallel potential (secondary x axis) along the spacecraft trajectory as a function of $\parallel$ position (y axis). (b) Electron distribution observed upstream. (c) Electron distribution observed downstream.

grating $J_\parallel E_\parallel$ along B_o, we find that the dissipation through the structure is $\sim$4 mW/m^2 and is equivalent to the inward directed transverse Poynting flux we measure on the edges of the cavity. Furthermore, at the cadence of the distribution measurements available on FAST, we do not find evidence for a discrete beam. Instead, we find that 96% of the observed current is carried by the field-aligned electron distribution at energies below 100 eV ($v < 6 \times 10^3$ km s^1 in Figures 2b and 2c) and at energies below those where the atmospheric loss cone is observed. These observations show that the majority of electromagnetic energy dissipated does not ultimately reside in the accelerated electron distribution and demonstrates that the observed current is carried by the bulk drift of the electron plasma along B_o.

[17] Having determined the parallel scale of the region containing $E_\parallel$, we now consider the magnitude of the parallel electric field that can be balanced by the convective derivative of equation (3) and that due to $\nabla_\parallel P_e$. Since the duration of $E_\parallel$ observation is of the order of 0.1 s, the total current due to the Alfvén wave can be assumed invariant over the observation time and over the 1.6-km parallel scale along B_o. This is because the interferometric results indicate Alfvén wave periods on the scale of the current > 1 s, and the Alfvén wave dispersion relation provides parallel wavelengths of at least 100 km for observed plasma parameters. In this approximation, the variation in $E_\parallel$ associated with the convective derivative from equation (3) becomes

$$\langle E_{\parallel v} \rangle \approx \frac{\mu_o \langle \lambda_e \rangle^2 \langle J_\parallel^2 \rangle}{q_e \langle n_e \rangle \Delta S_{\parallel ne}} \ln\left(\frac{n_e}{n_{eo}}\right) \tag{6}$$

where we hold $J_\parallel$ constant along B_o and so $\Delta S_{\parallel ne} \approx \Delta S_{\parallel v}$, where n_e is the density inside the cavity, n_{eo} is the density outside the cavity, and $\langle n_e \rangle = (n_e + n_{eo})/2$. Substituting the appropriate values from Figure 1, we find $\langle E_{\parallel v} \rangle = 10$ mV/m. With the assumption $\partial n_e/\partial S_\parallel \gg \partial T_e/\partial S_\parallel$, the parallel field balanced by the pressure gradient becomes

$$\langle E_{\parallel ne} \rangle \approx \frac{\langle T_e \rangle}{q_e \Delta S_{\parallel ne}} \ln\left(\frac{n_{eo}}{n_e}\right) \tag{7}$$

where $\langle T_e \rangle = (T_e + T_{eo})/2.0$. Since we find within the cavity that the density measured by the electron spectrometer on FAST lies within 50% of the density measured by the Langmuir probe, we obtain T_e from the appropriate velocity moment. Outside the cavity, T_{eo} cannot be reliably measured because most of the density lies below the 5-eV low energy limit of the detector and instead use $\langle T_e \rangle \geq T_e/2 = 15$ eV. Substituting these parameters, we find $\langle E_{\parallel ne} \rangle \geq -30$ mV/m. Averaging the observed field across the width of the cavity

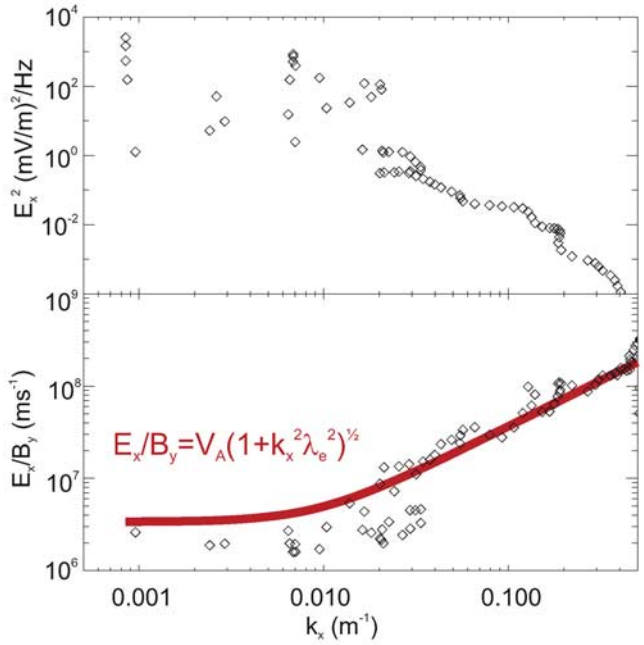

Figure 3. Spectral properties averaged over the interval shown in Figure 1. (a) Observed E_x^2 k-spectra. (b) Observed E_x/B_y and that expected for an inertial Alfvén wave (red) in the local approximation for measured V_A, n_e, and k_x.

where we measure n_e and n_{eo}, we find $\langle E_{||} \rangle \approx 30$ mV/m in agreement with the estimate from equation (7).

2.2. A Turbulent Spectrum of Alfvénic Fluctuations

[18] While we observe spectral peaks at frequencies close to f_{O+} suggesting the presence of ion cyclotron waves, most of the spectral energy density is contained in the broad spectrum of electromagnetic fluctuations observed coincident with the region of large $J_{||}$ and $E_{||}$. Broadband fluctuations over this frequency range are generally referred to as broadband extra low frequency noise (BBELF) [see, e.g., *Bonnell et al.*, 1996]. To demonstrate in this case that these fluctuations are consistent with inertial Alfvén waves, we determine $k_x(f_{sp})$ using a cross-spectral technique [*Labelle and Kintner*, 1989]. This analysis is based on the assumption that a single wave mode (or k) exists at each spacecraft frame frequency (f_{sp}) and is implemented using a wavelet-based interferometric technique applied to measurements from two electric field dipoles (5–6 and 7–8) separated by 55 m. The phase difference between the dipole pair can be expressed as $\phi(f_{sp}) = \phi_m(f_{sp}) + n2\pi$ where ϕ_m is the measured phase difference and $n = \pm1, \pm2, \pm3, \ldots$ is incremented by 1 whenever ϕ_m goes through $\pm\pi$ (antennae null). This occurs when the baseline length (55 m) becomes equal to an odd multiple of one-half wavelength projected along the baseline and allows us to resolve wave scales less than the baseline length. Once this phase difference is known, the wavelength along the baseline can be determined.

[19] Figure 3a shows the k_x spectra in E_x^2 for these fluctuations averaged over the interval shown in Figure 1. The variation in phase with spacecraft rotation (not shown) indicates that the phase fronts of the turbulent fields are almost parallel to B_o, and hence measured k is approximately k_x. A very similar result for $f_{sp} < 100$ Hz is obtained if it is assumed that f_{sp} is largely due to spacecraft Doppler shift and $k_x \approx 2\pi f_{sp}/v_{spacecraft}$. To demonstrate that these fluctuations are inertial Alfvén waves, we use the approach adopted by *Wahlund et al.* [1998] and *Stasiewicz et al.* [2000]. Figure 3b shows E_x/B_y spectra for the observations (diamonds) and the result expected for an inertial Alfvén wave (i.e., $E_x/B_y = V_A(1 + k_x^2\lambda_e^2)^{1/2}$, red line). The average density is $\sim$2000 cm^{-3} yielding $\lambda_e \sim 120$ m. From the locally observed dispersion of plasmaspheric hiss, we find that the plasma is composed of 90% O^+ [*Chaston et al.*, 1999] yielding an average Alfvén speed of $\sim 3.5 \times 10^6$ m s^1. With these observed parameters, the agreement between E_x/B_y observed and that expected for an inertial Alfvén wave provides evidence that these waves are inertial Alfvén waves. At smaller wave numbers (or larger scales), there is significant variation with the observed values generally more magnetic than expected for a travelling Alfvén wave. This is as may be expected above a conducting ionosphere [*Lysak*, 1998]. In fact, on these scales, the electric and magnetic field time series data shown in Figures 1b and 1d are $\sim$90° out of phase indicative of a standing wave and suggestive of the operation of the ionospheric Alfvén resonator or of a field line resonance.

3. Statistical Observations

[20] We have assembled a database of $\sim$7000 field-aligned current filaments with a peak $J_{||} \geq 10$ μA/m^2 estimated from the magnetic field data. These have been identified as Alfvén waves using the method described by *Chaston et al.* [2003] and have been included in the database only if high time resolution (80 ms) particle observations are simultaneously available. The magnitude of the observed upward current as a function of altitude is shown by the red line in Figure 4a where we also show in blue the averaged peak current measured over the width of the current filament by the electron analyzer experiment on FAST. The error bars represent 1 standard deviation. We find that $J_{||} \geq 100$ μA/m^2 comprise 2% of events and lie within 2 standard deviations of the average $J_{||}$. The black line shown in this panel is the expected altitude dependency for field-aligned currents which through $\nabla \cdot J = 0$ simply map with the geomagnetic field. The increasing separation between this line and the observed $J_{||}$ with decreasing altitude is indicative of the dissipation or reflection of the Alfvén wave as it propagates toward the ionosphere, as discussed in more detail for these observations by *Chaston et al.* [2003].

[21] Figure 4b shows the ratio of the lowest density measured across each current interval to the background density (as shown in Figure 4b) for each event. The color scale shows histograms as a function of altitude normalized by the total number of events in each altitude bin. The lowest scale (black) indicates <1 in every 50 events and the highest scale (red) shows greater that 1 in every 2 events as is indicated by the color bar. This provides a measure of the density variation across each current filament or an indication of cavity depth which as shown may vary from 0 to >90% (1% of events). The general trend indicates an increase in $\Delta n_e/n_e$ with increasing altitude with the distribution centered on 10–30% and 50% depletions at FAST

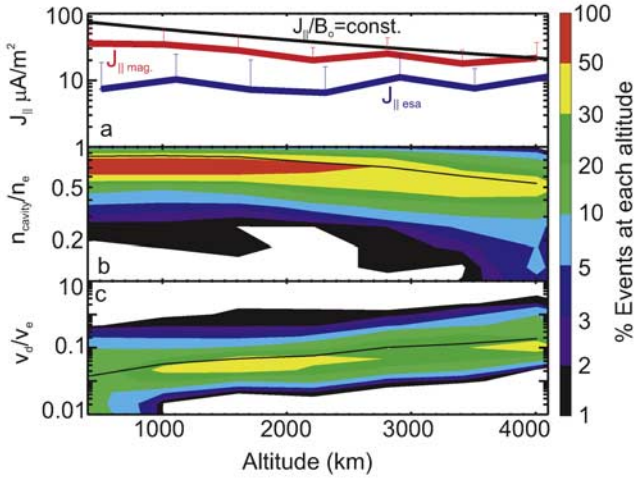

Figure 4. Some properties of large Alfvén wave currents from 350- to 4175-km altitude. (a) Field-aligned current in Alfvén waves as measured from Ampere's law applied to magnetometer measurements ($J_{\|mag}$, red) and from the electron analyzer ($J_{\|esa}$, blue). Black trace shows expected dependency without reflection or dissipation. (b) Cavity density normalized by background density. (c) Electron drift speed (v_d) required to carry the observed current normalized by the electron thermal speed (v_e) of the plasma within the cavity and above an energy of 5 eV or above the spacecraft potential.

perigee (z = 350 km) and apogee (z = 4175 km), respectively. Moreover, it is found that $\Delta n_e/n_e$ increases with $J_\|$ as shown in Figure 5a with $J_\| > 100$ μA/m^2 only observed in density depletions larger than 50%. Using these density measurements, we find that the observed width of the current filaments (Δx_j, i.e., the width of the region where the sign of $J_\|$ is constant) varies with $2\pi\lambda_e$ and is of the order of $2\pi\lambda_e$ averaged across the density cavity as shown in Figure 5b. Mapped with B_o to the ionosphere, these widths have an average value of $\sim$1 km.

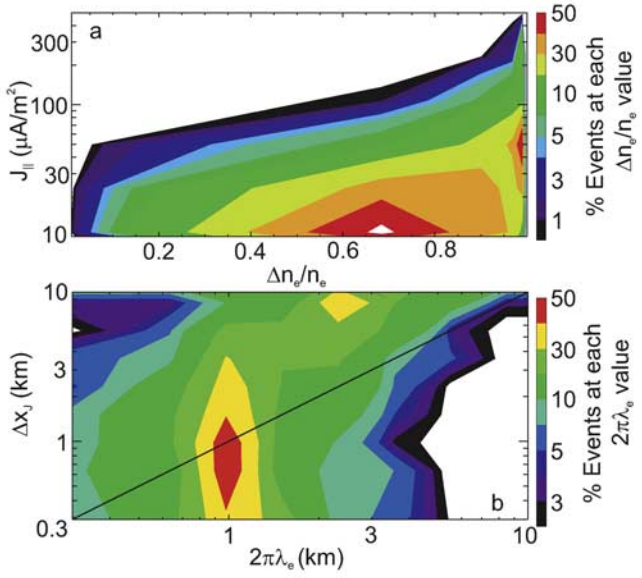

Figure 5. (a) Observed current density against density cavity depth. (b) Observed current filament width against $2\pi\lambda_e$ averaged across the cavity. The color scale shown is the percentage of events in each $\Delta n_e/n_e$ and $2\pi\lambda_e$ bin (the total % at each abscissa value is 100%).

[22] Figure 4c shows the peak value of v_d/v_e across each Alfvénic current filament. This ratio is based on the temperature measurement closest to the lowest density point across the filament and the electron drift required to carry the observed current measured from the magnetometer at that time. The value of v_e is based on the velocity moment taken above the spacecraft potential in the cavity and so, except in those cases where all the cold ionospheric plasma has been depleted, represents an overestimate. Consequently these values show the lower limit for v_d/v_e. From these measurements, it is generally found that $v_d/v_e \geq 0.1$, and for 2.1% of events, we find $v_d/v_e \geq 1.0$. These results are similar to the measurements reported by *Ergun et al.* [1999] found in electron solitary structures. Given the strong instability that occurs as $v_d \rightarrow v_e$, $v_d < v_e$ is an expected result. However, as shown by several simulation studies [*Newman et al.*, 2001; *Singh*, 2002], the result that on average $v_d/v_e \geq 0.1$ suggests that double layers may be a commonly occurring feature in Alfvén wave currents above the aurora.

[23] In Figure 6, we plot the field-aligned potential due to the electron inertia as given by equation (6) against that due the electron pressure gradient given by equation (7). These data include only those events where the density observed by the electron spectrometer inside the cavity is within 50% of that derived from the Langmuir probe. This ensures that our estimate for the electron plasma temperature derived from the first-order moment of the electron distribution within the cavity is meaningful. We find potentials through these features which may be as large as 1 keV with the majority between 10 and 100 eV. Those points below the

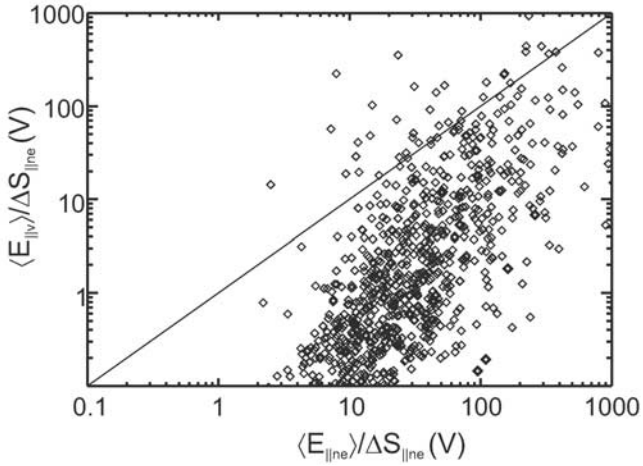

Figure 6. Field-aligned potentials due to electron pressure gradients ($\langle E_{\|ne}\rangle/\Delta S_{\|ne}$) as given by equation (7) plotted against those that due to electron inertia ($\langle E_{\|v}\rangle/\Delta S_{\|ne}$) as given by equation (6). Data points above the diagonal line are those where $|E_{\|v}| > |E_{\|ne}|$. Only those events where the density measured by the electrostatic analyzer is within 50% of the density measured by the Langmuir probe are included.

diagonal line in this plot show those events where, according to equations (6) and (7), electron pressure gradients provide the dominant potential drop through these structures. These account for 95% of the ensemble of events observed. Since from equations (6) and (7) both $\langle E_{\parallel ne}\rangle$ and $\langle E_{\parallel} v\rangle$ vary equally with the magnitude of the density gradient, these results indicate that the large parallel electric fields sometimes observed in density cavities with Alfvénic upward currents are primarily supported by the electron pressure gradients they contain. For $\Delta S_{\parallel ne} \sim$ kilometers (as found in the case study example), these potentials will be associated with $E_{\parallel} \sim 1-1000$ mV/m.

4. Discussion

4.1. Comparison With Observations From the Freja Satellite

[25] Case study examples of large field-aligned currents, density depletions, and parallel electric fields in Alfvén waves have been reported previously from the Freja satellite [*Stasiewicz et al.*, 1997, 1998; *Chust et al.*, 1998]. These authors identify current magnitudes typically of the order of 50 μA/m^2 [*Chust et al.*, 1998] in these structures and in exceptional cases up to 300 μA/m^2 [*Stasiewicz et al.*, 1997]. The local density depletions observed coincident with these currents extend up to ~90% of the background density, and parallel fields in excess of 100 mV/m are observed. It is speculated by *Chust et al.* [1998] that such fields may be double layers. Without statistical measurements of these features from Freja, a rigorous comparison with those observed from FAST cannot be performed. However, the values reported by these authors are all consistent with the ensemble we measure from FAST as documented in this report.

4.2. Double Layer Formation in Alfvén Waves

[26] These results suggest a scenario whereby current filamentation/localization in Alfvén waves leads to the formation of double layers and density cavities in a manner similar to that proposed by *Mishin and Forster* [1995]. While these processes tend to promote one another, observations suggest that wave reflection from the ionosphere may play a crucial role. From a survey of a number of such events, we find that in general, an ~90° phase difference exists between E_x and B_y across the density depletion where the peak in current occurs. Apart from indicating that this feature is not just a stationary field-aligned current, it is indicative of the superposition of an incident and reflected wave or of a standing Alfvén wave. *Lysak and Dum* [1983] demonstrated that the superposition of an incident and reflected Alfvén wave from the ionosphere could lead to intensification of $J_{\parallel}$ over transverse scales of the order of electron inertial lengths. Significantly, this is the most commonly found transverse scale of $J_{\parallel}$ we observe. This work has recently been extended by *Lysak and Song* [2002] to show how currents >10 μA/m^2 over transverse scales of $2\pi\lambda_e$ arise from broader current structures because of the nonlinear evolution of the ionospheric feedback instability. In a related study, *Streltsov and Lotko* [2004] have demonstrated how such structures may form through the feedback instability on the same scales that we observe provided the ionospheric conductivity is similar to the Alfvén conductivity in the magnetosphere. Once transverse scales of $\sim 2\pi\lambda_e$ have been reached, it has been shown by *Seyler* [1990] from three-dimensional fluid simulations how the current may decay to form a turbulent spectrum of inertial Alfvén waves as we observe. This process has recently been attributed to a current convective instability [*Seyler and Xu*, 2003] operating on transverse scales of $2\pi\lambda_e$. Together these models provide a plausible means, supported by observations, through which large-scale currents may cascade to the smaller-scale features we observe where density cavities and double layers can form.

[27] The formation of the density cavity may occur naturally as part of the localization of the wave current and the generation of the turbulent inertial Alfvén waves. Various models have shown how the ponderomotive force in shear Alfvén waves on small scales can lead to density depletions [*Bellan and Stasiewicz*, 1998; *Shukla and Stenflo*, 1999]. *Lu et al.* [2003] have demonstrated how coupling of the shear mode on transverse scales of the order of $2\pi\lambda_e$ to the slow mode can lead to density fluctuations and cavity formation. Observations (including the case study we show in this report) show transverse wave Poynting fluxes directed inward toward the center of the density depletion [*Chaston et al.*, 2006], indicating that the Alfvén wave energy is focused into the cavity. The focusing of shear Alfvén waves due to transverse shear Alfvén phase speed gradients that these depletions provide has been demonstrated over small parallel scales using particle-in-cell (PIC) simulations [*Genot et al.*, 2004] and globally through analytical theory and fluid simulations by *Rankin et al.* [2005]. At some point, ion heating within these cavities will occur, either through direct interaction with the small-scale inertial Alfvén waves [*Stasiewicz*, 2000] or via plasma waves driven unstable by the increasing wave current. It has been shown from modeling [*Singh*, 1992, 1994] and from observations [*Chaston et al.*, 2006] that these waves may lead to accelerated erosion of the plasma within the cavity. These processes serve to reinforce one another in such a way that density irregularities in the auroral ionosphere are unstable to incoming Alfvén wave Poynting flux and will require increasingly larger values of v_d to carry wave current as the erosion of plasma within the cavity continues.

[28] If these processes can eventually provide current densities of magnitude $J_{\parallel} \approx (n_e q_e)(2T_e/m_e)^{1/2}$ (or $v_d \approx v_e$), then according to the analysis of *Block* [1972], strong double layers can be expected to form. That this may occur in Alfvén waves above the aurora was demonstrated by *Silberstein and Otani* [1994] and *Genot et al.* [2004] using PIC simulations. Vlasov simulations performed by *Newman et al.* [2001] and *Singh* [2002, 2003] show dynamically how current-driven double layers, as can be expected in Alfvén waves, lead to depletions up to 80% from an initial "seed" density depression of ~10–30%. These authors show that the ratio of v_d/v_e decreases with time through electron heating once the double layer has formed and with distance downstream from the layer. These variations may account for the result that v_d/v_e we observe is generally less than 1, yet still be consistent with the presence of double layers.

[29] Whatever the exact process by which the cavities form, they are necessary for the formation of large (>10 mV/m) $E_{\parallel}$ in Alfvén waves which can be expected

to be observed in association with large Alfvénic $J_{\|}$ whenever the electron density is sufficiently small that $v_d \rightarrow v_e$. This study has shown that this condition is achieved in Alfvén waves above the aurora and more generally that large (>10 mV/m) $E_{\|}$ observed in Alfvén waves currents can be balanced by $\nabla_{\|}P_e$.

5. Conclusion

[30] We have reported case study and statistical measurements over the altitude range from 350 to 4175 km of intense filamentary Alfvénic field-aligned currents (>10 μA/m^2) embedded in density depletions or cavities in which large $E_{\|}$ (>10 mV/m) is sometimes observed above the auroral oval. We find cavity depths for 1% of events larger than 90% but typically from 30% to 50% and wave currents in excess of 100 μA/m^2 for 2% of events. The magnitude of the wave current is shown to increase with cavity depth, and the width of the current filaments is shown to be $\sim 2\pi\lambda_e$. It has been shown that for at least 2.1% of events, the Bohm criterion in the fluid approximation for the existence of double layers inside these Alfvénic cavities is satisfied. For a subset of the database where accurate measurements of the temperature inside the cavities can be obtained, we have shown that field-aligned electron pressure gradients manifest through the gradients in density provide a plausible means for supporting the large parallel electric fields observed. These observations together suggest that the large amplitude parallel electric fields found embedded in these Alfvénic cavities exist as double layers through which the FAST spacecraft occasionally passes.

Appendix A

[31] Measurement of the velocity of the parallel electric field structure is achieved using dipole measurements of the electric field made between spheres 5–6 and 7–8 and spacecraft-sphere potential measurements using spheres 1 and 4 as shown in Figure 1a. These provide two orthogonal baselines in the spin plane which lies within 2.4° of B_o. The approximate speed of the structure in the spacecraft frame in a geomagnetic field-aligned coordinate system can then be found by the solution of the equation $\mathbf{v}_B = \mathbf{R}^1\mathbf{v}_{sp}$. Here $\mathbf{R}$ is the 2×2 matrix with each row defined by $\mathbf{r}_j/r_j$ where $\mathbf{r}_j$ is the vector pointing along each baseline j in the field-aligned coordinate system. $\mathbf{v}_{sp}$ is the vector of observed velocities along each baseline given by the time delay between measurements made along each baseline divided by its length.

[32] **Acknowledgments.** This research was supported by NASA grants NAG-12453, NAG-3596, NAG-127984, and NAG-12954. Chris Chaston is indebted to Brian Fraser and to the University of Newcastle where much of this work was completed.

[33] Wolfgang Baumjohann thanks Robert Lysak and another reviewer for their assistance in evaluating this paper.

References

Andersson, L., R. E. Ergun, D. L. Newman, J. P. McFadden, and C. W. Carlson (2002), Characteristics of parallel electric fields in the downward current region of the aurora, *Phys. Plasmas*, *9*, 3600.

Bellan, P., and K. Stasiewicz (1998), Fine scale cavitation of ionospheric plasma caused by inertial Alfvén wave ponderomotive force, *Phys. Rev. Lett.*, *80*, 3523.

Block, L. (1972), in *Earth's Magnetospheric Processes*, ed. B. M. McCormac, p. 258, Springer, New York.

Bonnell, J., P. Kintner, J. E. Wahlund, K. Lynch, and R. Arnoldy (1996), Interferometric determination of broadband ELF wave phase velocity within a region of transverse auroral ion acceleration, *Geophys. Res. Lett.*, *101*, 5279.

Chaston, C. C., C. W. Carlson, W. J. Peria, R. E. Ergun, and J. P. McFadden (1999), FAST observations of inertial Alfvén waves in the dayside aurora, *Geophys. Res. Lett.*, *26*, 647.

Chaston, C. C., C. W. Carlson, R. E. Ergun, J. P. McFadden, and R. J. Strangeway (2003), Properties of small-scale Alfvén waves and accelerated electrons from FAST, *J. Geophys. Res.*, *108*,(A4) 8003, doi:10.1029/2002JA009420.

Chaston, C. C., V. Genot, J. W. Bonnell, C. W. Carlson, J. P. McFadden, R. E. Ergun, R. J. Strangeway, E. J. Lund, and K. J. Hwang (2006), Ionospheric erosion by Alfvén waves, *J. Geophys. Res.*, *111*, A03206, doi:10.1029/2005JA011367.

Chust, T., P. Louarn, M. Volwerk, H. De Feraudy, A. Roux, J.-E. Wahlund, and B. Holback (1998), Electric fields with a large parallel component observed by Freja spacecraft: Artifacts or real signals?, *J. Geophys. Res.*, *103*, 215.

Ergun, R. E., et al. (1998), FAST satellite observations of electric field structures in the auroral zone, *Geophys. Res. Lett.*, *25*, 2025.

Ergun, R. E., C. W. Carlson, L. Muschietti, I. Roth, and J. P. McFadden (1999), Properties of fast solitary structures, *Nonlinear Process. Geophys.*, *6*, 187.

Ergun, R. E., L. Andersson, Y.-J. Su, D. L. Newman, M. V. Goldman, W. Lotko, C. C. Chaston, and C. W. Carlson (2005), Localized parallel electric fields associated with inertial Alfvén waves, *Phys. Plasmas*, *12*, 072901.

Genot, V., P. Louarn, and F. Mottez (2004), Alfvén wave interaction with inhomogeneous plasmas: Acceleration and energy cascade toward smaller scales, *Ann. Geophys.*, *22*, 931.

Hasegawa, A. (1976), Particle acceleration by MHD surface wave and formation of aurora, *J. Geophys. Res.*, *81*, 5083.

Hull, A. J., W. Bonnell, F. S. Mozer, J. D. Scudder, and C. C. Chaston (2003), Large parallel electric fields in the upward current region of the aurora: Evidence for ambipolar effects, *J. Geophys. Res.*, *108*(A6), 1265, doi:10.1029/2002JA009682.

Labelle, J., and P. M. Kintner (1989), The measurement of wavelength in space plasmas, *Rev. Geophys.*, *27*, 495.

Lu, J.Y., R. Rankin, R. Marchand, V. T. Tikhonchuk, and J. Wanliss (2003), Finite element modeling of nonlinear dispersive field line resonances: Trapped shear Alfvén waves inside field-aligned density structures, *J. Geophys. Res.*, *108*(A11), 1394, doi:10.1029/2003JA010035.

Lysak, R. L. (1998), The relationship between electrostatic shocks and kinetic Alfvén waves, *Geophys. Res. Lett.*, *25*(12), 2089–2092, doi:10.1029/98GL00065.

Lysak, R. L., and C. W. Carlson (1981), Effect of microturbulence on magnetosphere-ionosphere coupling, *Geophys. Res. Lett.*, *8*, 269.

Lysak, R. L., and C. T. Dum (1983), Dynamics of magnetosphere-ionosphere coupling including turbulent transport, *J. Geophys. Res.*, *88*, 365.

Lysak, R. L., and X. Lotko (1996), On the kinetic dispersion relation for shear Alfvén waves, *J. Geophys. Res.*, *101*, 5085.

Lysak, R. L., and Y. Song (2002), Energetics of the ionospheric feedback interaction, *J. Geophys. Res.*, *107*(A8), 1160, doi:10.1029/2001JA000308.

Lysak, R. L., and Y. Song (2003), Non-local kinetic theory of Alfvén waves on dipolar field lines, *J. Geophys. Res.*, *108*(A8), 1327, doi:10.1029/2003JA009859.

Mishin, E. V., and M. Forster (1995), Alfvénic shocks and low altitude auroral acceleration, *Geophys. Res. Lett.*, *22*, 1745.

Newman, D. L., M. V. Goldman, R. E. Ergun, and A. Mangeney (2001), Formation of double layers and electron holes in a current-driven space plasma, *Phys. Rev. Lett.*, *87*, doi:10.1103/PhysRevLett.87.255001.

Raadu, A., and J. Rasmussen (1988), Dynamical aspects of electrostatic double layers, *Astrophys. Space Sci.*, *144*, 43.

Rankin, R., J. C. Samson, and V. T. Tikhonchuk (1999), Parallel electric fields in dispersive shear Alfvén waves in the dipolar magnetosphere, *Geophys. Res. Lett.*, *26*, 3601.

Rankin, R., R. Marchand, J. Y. Lu, K. Kabin, and V. T. Tikhonchuk (2005), Theory of dispersive shear Alfvén wave focusing in Earth's magnetosphere, *Geophys. Res. Lett.*, *32*, L05102, doi:10.1029/2004GL021831.

Ronnmarck, K., and M. Hamrin (2000), Auroral electron acceleration by Alfvén waves and electrostatic fields, *J. Geophys. Res.*, 25333.

Seyler, C. E. (1990), A mathematical model of the structure and evolution of small scale discrete auroral arcs, *J. Geophys. Res.*, *95*, 17199.

Seyler, C., and T. Xu (2003), The relationship between field-aligned currents and low frequency electromagnetic fluctuations, *Geophys. Res. Lett.*, *30*(21), 2106 doi:10.1029/2003GL018292.

Seyler, C.-E., J.-E. Wahlund, and B. Holback (1995), Theory and simulation of low-frequency plasma waves and comparison to Freja satellite observations, *J. Geophys. Res.*, *100*, 21453.

Shukla, P., and L. Stenflo (1999), Plasma density cavitation due to inertial Alfvén wave heating, *Phys. Plasmas*, *6*, 4120.

Silberstein, M., and N. F. Otani (1994), Computer simulation of Alfvén waves and double layers along auroral field lines, *J. Geophys. Res.*, *99*, 6351.

Singh, N. (1992), Plasma perturbations created by transverse ion heating events in the magnetosphere, *J. Geophys. Res.*, *97*, 4235.

Singh, N. (1994), Pondermotive versus mirror force in creation of the filamentary cavities in the auroral plasma, *Geophys. Res. Lett.*, *21*, 257.

Singh, N. (2002), Spontaneous formation of current-driven double layers in density depletions and its relevance to solitary Alfvén waves, *Geophys. Res. Lett.*, *29*(7), 1147, doi:10.1029/2001GL014033.

Singh, N. (2003), Dynamically evolving double layers and density depletions, *J. Geophys. Res.*, *108*(A8), 1322, doi:10.1029/2002JA009815.

Song, Y., and R. L. Lysak (2006), Displacement current and the generation of parallel electric fields, *Phys. Rev. Lett.*, *96*, 145002.

Stasiewicz, K. (2000), Stochastic ion heating by orbit chaotization on electrostatic waves and non-linear structures, *Phys. Scr.*, *T-84*, 60.

Stasiewicz, K., G. Gustaffson, G. Marklund, P.-A. Lindqvist, J. Clemmons, and L. Zanetti (1997), Cavity resonators and Alfvén resonance cones observed on Freja, *J. Geophys. Res.*, *102*, 2565.

Stasiewicz, K., G. Holmgren, and L. Zanetti (1998), Density depletions and current singularities observed by Freja, *J. Geophys. Res.*, *103*, 4251.

Stasiewicz, K., Y. Khotyaintsev, M. Berthomier, and J.-E. Wahlund (2000), Identification of widespread turbulence of dispersive Alfvén waves, *Geophys. Res. Lett.*, *27*, 173.

Streltsov, A. V., and W. Lotko (2004), Multiscale electrodynamics of the ionosphere-magnetosphere system, *J. Geophys. Res.*, *109*, A09214, doi:10.1029/2004JA010457.

Streltsov, A. V., W. Lotko, A. Keiling, and J. R. Wygant (2002), Numerical modeling of Alfvén waves observed by the Polar spacecraft in the nightside plasma sheet boundary layer, *J. Geophys. Res.*, *107*(A8), 1173 doi:10.1029/2001JA000233.

Thompson, B. J., and R. L. Lysak (1996), Electron acceleration by inertial Alfvén waves, *J. Geophys. Res.*, *101*, 5359.

Vedin, J., and K. Ronnmarck (2005), Electron pressure effects on driven auroral Alfvén waves, *J. Geophys. Res.*, *110*, A01214, doi:10.1029/2004JA010610.

Wahlund, J.-E., et al. (1998), Broadband ELF plasma emission during auroral energisation, 1, Slow ion acoustic waves, *J. Geophys. Res.*, *103*, 4343.

Wright, A. N., W. Allan, M. S. Rudermann, and R. C. Elphic (2002), The dynamics of current carriers in standing Alfvén waves: Parallel electric fields in the auroral acceleration region, *J. Geophys. Res.*, *107*(A7), 1120, doi:10.1029/2001JA900168.

J. W. Bonnell, C. W. Carlson, C. C. Chaston, A. J. Hull, and J. P. McFadden, Space Physics Research Group, Space Sciences Laboratory, University of California, Berkeley, Cetennial Drive at Grizzly Peak Boulevard, Berkeley, CA 94720-7450, USA. (ccc@ssl.berkeley.edu)

R. E. Ergun, Laboratory for Atmospheric and Space Physics, University of Colorado, Boulder, CA, USA.

R. J. Strangeway, Institute for Geophysical and Planetary Physics, University of California, Los Angeles, Los Angeles, CA, USA.